Available online at www.sciencedirect.com
ScienceDirect
Journal of Photochemistry and Photobiology A: Chemistry 190 (2007) 359–371
Journal of Photochemistry and Photobiology A:Chemistry
www.elsevier.com/locate/jphotochem

Laser control in open molecular systems: STIRAP and Optimal Control

D. Sugny [a], M. Ndong [b,c], D. Lauvergnat [b,c], Y. Justum [b,c], M. Desouter-Lecomte [b,c,d,*]

[a] *Laboratoire de Physique de l'Université de Bourgogne, Unité Mixte de Recherches 5027 CNRS et Université de Bourgogne, BP 47870, 21078 Dijon, France*
[b] *Univ Paris-Sud, Laboratoire de Chimie Physique, UMR8000, Orsay F-91405, France*
[c] *CNRS, Laboratoire de Chimie Physique, UMR0000, Orsay F-91405, France*
[d] *Département de Chimie, Université de Liège, Institut de Chimie B6, Sart-Tilman B-4000, Liège 1, Belgium*

Available online 6 December 2006

Abstract

We examine the effect of dissipation on the laser control of a process that transforms a state into a superposed state. We consider a two-dimensional double well of a single potential energy surface. In the context of reactivity, the objective of the control is the localization in a given well, for instance the creation of an enantiomeric form whereas for quantum gates, this control corresponds to one of the transformation of the Hadamard gate. The environment is either modelled by coupling few harmonic oscillators (up to five) to the system or by an effective interaction with an Ohmic bath. In the discrete case, dynamics is carried out exactly by using the coupled harmonic adiabatic channels. In the continuous case, Markovian and non-Markovian dynamics are considered. We compare two laser control strategies: the Stimulated Raman Adiabatic Passage (STIRAP) method and the optimal control theory. Analytical estimations for the control by adiabatic passage in a Markovian environment are also derived.

Keywords: STIRAP; Optimal control; Hadamard gate; Qubit; Dissipative dynamics; Markovian and non-Markovian dynamics; Coupled adiabatic channels

1. Introduction

Controllability of wave packets in a double-well potential has been largely explored since the early days of laser-driven dynamics and remains nowadays an attractive topic [1]. Symmetric or asymmetric double wells are ubiquitous in chemical physics and can be encountered in the context of hydrogen tunneling, electron transfer and isomerization or enantiomer separation. According to the barrier height and the corresponding tunneling time, the control aims at transferring a wave packet from one well to the other [2–11] or at localizing a delocalized state in a given well [12–15]. A large number of model systems have already been investigated, we can cite for example the selective preparation of enantiomer in H_3POSH [13], the intramolecular hydrogen transfer in malonalhehyde [2] and thioacetone [5], the Cope rearrangement in semibullvalene [3], the control of molecular chirality in difluoro[*c*]phenanthrene [10] and the isomerization of hydrogen cyanide [16–21] or methoxy radical [31]. Recently, the exciting new field of molecular quantum computing has emerged and vibrational states have been proposed to be a potential candidate for implementing quantum qubits [22–28]. Vibrational states of a double-well system have been used for that purpose [29–31]. The goal of quantum control is to design laser pulses able to drive a quantum system towards a specified target state whereas in the context of quantum computation, the goal is the implementation of unitary transformations acting on different inputs. This latter control is thus more challenging due to multiple initial states and corresponding targets and more demanding about the performance of the control.

In this paper, we propose to revisit the control of a double-well system by gathering two different strategies: the Stimulated Raman Adiabatic Passage (STIRAP) scheme and the Optimal Control Theory (OCT). We address the fundamental problem of the control of this system when is coupled with an environment. We do not consider non-adiabatic interactions between different energy surfaces in this work. We compare the efficiency of STIRAP and OCT by analyzing the structure and the robustness of the pulses obtained and their characteristics (intensity, duration) needed to achieve different objectives. We choose a two-dimensional (2D) potential energy surface modeling the migration of a hydrogen atom around a CO bond (isomerization $H_3CO \rightarrow H_2COH$). This is a benchmark case for a surface presenting three wells connected by a bifurcating region. We

* Corresponding author. Tel.: +33 169158146; fax: +33 169154447.
E-mail address: mdesoute@lcp.u-psud.fr (M. Desouter-Lecomte).

1010-6030/$ – see front matter © 2007 Elsevier B.V. All rights reserved.
doi:10.1016/j.jphotochem.2006.12.005

notice that this 2D surface exhibits symmetric and asymmetric double-wells allowing various wave packet controls. The dynamically active coordinates are two angles (spherical coordinates of the migrating atom with respect to the middle of the bond). It is clear that consideration of other degrees of freedom or more generally coupling with an environment will be crucial in laser driven dynamics. The point is to increase the number of dynamically active degrees of freedom or to simulate dynamics in condensed phase by efficient and realistic dissipative models [32,33]. In a first approach, we consider the coupling of the active modes with a small number of bath oscillators. Dynamics is treated in the framework of coupled adiabatic channels which allow considering exactly up to seven degrees of freedom. It should be also possible to use alternative approaches, for example the promising OCT-MCTDH (Multiconfiguration Time-Dependent Hartree) method [34] which can take into account a larger number of oscillators [35,36], particularly with the G-MCTDH extension which uses Gaussian wave packets for some modes [37] or the surrogate Hamiltonian method [38]. In a second step, we simulate the remaining intra-molecular modes and the degrees of freedom of the surrounding environment by a bath with an Ohmic spectral density. We consider the control of a non-Markovian dynamics by an efficient extension [39] of the Rabitz iterative methods used to solve OCT equations in the density matrix formulation [40]. We neglect correlation between dissipation and laser-driven dynamics [41,42]. Alternative methods could also be used to treat the dissipative memory kernel [43]. Another approach using STIRAP scheme [44,45] has been implemented in the case of a Markovian dynamics [46–49]. We do not use STIRAP strategy in a purely adiabatic regime which requires pulses of large duration. In order to reduce this time, we consider the solution given by the adiabatic equations as a trial field depending on several parameters as the Rabi frequencies. In a second step, we optimize the different parameters to keep efficient control. Note that OCT can be viewed as a control scheme optimizing a laser field with an infinity of degrees of freedom, which justifies the comparison between the two methods. Finally, we point out that different mixed quantum-classical approaches based on the hydrodynamical description [50] or on Wigner distribution [51] are promising issues for laser driven dynamics of complex systems.

2. Dissipative dynamics

The total Hamiltonian (system + bath) can be written as

$$\hat{H} = \hat{H}_0^{\mathrm{ND}} + \hat{H}_{\mathrm{Field}} + \sum_j^{N_b} \left[\frac{\hat{P}_j^2}{2_j} + \frac{1}{2}\omega_j^2 \left(Q_j - \frac{c_j f(\mathbf{q})}{\omega_j^2} \right)^2 \right] \tag{1}$$

where $\hat{H}_0^{\mathrm{ND}}$ is here a 2D double-well Hamiltonian, $\hat{H}_{\mathrm{Field}} = -\vec{\mu}\vec{E}(t)$ and $\mathbf{q}$ are the active coordinates coupled to the bath. This Hamiltonian contains a bath Hamiltonian expressed in mass weighted coordinates

$$\hat{H}_{\mathrm{B}} = \sum_j^{N_b} \frac{\hat{P}_j^2}{2_j} + \frac{1}{2}\omega_j^2 Q_j^2 \tag{2}$$

and a system Hamiltonian which includes a renormalization term

$$\hat{H}_{\mathrm{S}} = \hat{H}_0^{\mathrm{ND}} + \hat{H}_{\mathrm{Field}} + \hat{H}_{\mathrm{renorm}} \tag{3}$$

with

$$\hat{H}_{\mathrm{renorm}} = \frac{1}{2} f(\mathbf{q})^2 \sum_{j=1}^{N_b} \frac{c_j^2}{\omega_j^2} \tag{4}$$

This leads to a system bath coupling of the form

$$\hat{H}_{\mathrm{SB}} = -f(\mathbf{q}) \sum_j^{N_b} c_j Q_j \tag{5}$$

We compare two situations: one in which the system is coupled with few modes (up to five) and another in which it is coupled to a continuous distribution of oscillators. In the latter case, the coupling constants are characterized by the following bath spectral density (Caldeira Legett model [52])

$$J(\omega) = \frac{\pi}{2} \sum_j^{N_b} \frac{c_j^2}{\omega_j} \delta(\omega - \omega_j) \quad \text{and} \quad J(-\omega) = -J(\omega). \tag{6}$$

This density is approximated by an Ohmic function

$$J(\omega) = \lambda^2 \frac{\omega}{\omega_c} \mathrm{e}^{-|\omega|/\omega_c} \tag{7}$$

where ω_c is the reference frequency corresponding to the maximum of the function.

In the case of a finite number of oscillators, the bath spectral density is discretized by

$$c_j^2 = \frac{2}{\pi} \omega_j \frac{J(\omega_j)}{d(\omega_j)} \tag{8}$$

where $d(\omega)$ is the frequency density which is estimated by

$$d(\omega) = \frac{N_b}{\omega_c} \frac{\mathrm{e}^{-\omega/\omega_c}}{1 - \mathrm{e}^{-\omega_m/\omega_c}}, \tag{9}$$

ω_m being the largest frequency of the bath [35].

In the case of an infinite ensemble of oscillators, the system density matrix is defined by $\rho(t) = \mathrm{Tr}_{\mathrm{B}} \sigma_{\mathrm{S}\oplus\mathrm{B}}(t)$ where Tr_{B} is the partial trace over the bath degrees of freedom. The reduced evolution equation for $\rho(t)$ is obtained in the framework of the projector formalism of Zwanzig–Nakajima [32,33,53]. Different approximations are made to derive the operational equations. Initial correlation between the system and bath degrees of freedom is neglected, i.e. the initial density matrix factorizes as $\sigma_{\mathrm{S}\oplus\mathrm{B}}(t=0) = \rho(t=0)\rho_{\mathrm{B}}^{\mathrm{eq}}$ and the bath is assumed to be in thermal equilibrium. Initial correlation could be introduced by using a more sophisticated treatment [54]. As mentioned above, we also neglect the correlation between the laser and the dissipation dynamics [41,42]. The second order expansion of the

Table 1
Half-live time $\tau_{1/2}$ in fs and the time τ_{max} for which $C(t)$ (Eq. (12)) vanishes for the two reference frequencies (Eq. (7)) and temperatures used in the simulations

	$\omega_c = 1000\,\mathrm{cm}^{-1}$	$\omega_c = 400\,\mathrm{cm}^{-1}$	$\omega_c = 100\,\mathrm{cm}^{-1}$
$T = 298$ K	$\tau_{1/2} = 3$, $\tau_{max} = 50$	$\tau_{1/2} = 9$, $\tau_{max} = 200$	$\tau_{1/2} = 50$, $\tau_{max} = 500$
$T = 100$ K	$\tau_{1/2} = 2.8$, $\tau_{max} = 47$	$\tau_{1/2} = 7$, $\tau_{max} = 80$	$\tau_{1/2} = 38$, $\tau_{max} = 400$

exact Zwanzig–Nakajima reduced equation in the Schrödinger representation reads [3,32]

$$\frac{\partial \rho_{kl}(t)}{\partial t} = -i\frac{\varepsilon_k - \varepsilon_l}{\hbar}\rho_{kl}(t) + \frac{i}{\hbar}\sum_j E_j(t)[\mu_j, \rho(t)]_{kl} - \frac{1}{\hbar^2}[A, G(t)]_{kl} \tag{10}$$

with a memory

$$G_{kl}(t) = \int_0^t \mathrm{d}\tau\, \mathrm{e}^{-i\omega_{kl}\tau}\{C(\tau)[A\rho(t-\tau)]_{kl} - C(-\tau)[\rho(t-\tau)A]_{kl}\} \tag{11}$$

where A is the matrix of the function of the active coordinate $f(\mathbf{q})$ (Eq. (4)). The bath correlation function is given by [41]

$$C(t \geq 0) = \frac{1}{\pi}\int_{-\infty}^{\infty} \mathrm{d}\omega\, \mathrm{e}^{-i\omega t}\frac{J(\omega)}{1 - \mathrm{e}^{-\beta\omega}} \quad \text{and} \quad C(-t) = C^*(t). \tag{12}$$

where $\beta = 1/kT$ is the Boltzmann factor. The coupling strength with the bath λ finally appears in the memory as λ^2. The Markov approximation consists in replacing the upper born of integration in Eq. (11) by $t = \infty$ and $\rho(t-\tau)$ by $\rho(t)$. Different approximations such as a rotating wave approximation then lead to the Redfield [55] or the Lindblad form [32,33,56,57]. We recall that the Markovian regime arises when the correlation time of the bath τ_B is smaller than the typical time scale τ_S over which the system varies appreciably. We choose the Lindblad form because it can be shown that the density matrix of the system ρ remains a positive semi-definite Hermitian operator having $\mathrm{Tr}[\rho] = 1$ and $\mathrm{Tr}[\rho^2] \leq 1$. Here, the Lindblad equations take the form:

$$\begin{aligned}
\dot{\rho}_{kl} &= -i\frac{\varepsilon_k - \varepsilon_l}{\hbar} + \frac{i}{\hbar}\sum_j E_j(t)[\mu_j, \rho(t)]_{kl} \\
&\quad + \sum_m -\frac{1}{2}[\gamma(\omega_{mk})|A_{mk}|^2 + \gamma(\omega_{ml})|A_{ml}|^2]\rho_{kl}, \\
\dot{\rho}_{kk} &= +\frac{i}{\hbar}\sum_j E_j(t)[\mu_j, \rho(t)]_{kk} \\
&\quad + \sum_m [\gamma(\omega_{km})|A_{km}|^2\rho_{mm} - \gamma(\omega_{mk})|A_{mk}|^2\rho_{kk}]
\end{aligned} \tag{13}$$

where

$$\gamma(\omega) = \frac{J(\omega)}{1 - \mathrm{e}^{-\beta\omega}} \tag{14}$$

In this paper, we examine the effect of the system-bath interaction on the laser control. We vary the reference frequency ω_c (Eq. (7)) and the temperature ($T = 298$ and 100 K) and therefore the correlation function $C(t)$ (Eq. (12)) which determines the memory time. The characteristic time scale of the bath τ_B may be estimated by the half-life time $\tau_{1/2}$ and also by the time τ_{max} for which $C(t)$ vanishes. The two $\tau_{1/2}$ and τ_{max} times are given in fs in Table 1.

We summarize the three relevant time scales. τ_B is typically of the order of 10 fs, τ_S is about 50 fs when it is estimated by a typical frequency of $600\,\mathrm{cm}^{-1}$ but the tunneling time reaches 50 ps. The relaxation time τ_R is roughly given by $1/\lambda^2$, i.e. about 6 ps for most of our examples using $\lambda = 2 \times 10^{-3}$. We will consider different situations for which non-Markovian dynamics is justified because τ_B is not smaller than τ_S.

3. Model

The model represented in Fig. 1 is a bifurcating region in the ground potential energy surface of a polyatomic system (isomerization $H_3CO \rightarrow H_2COH$). Such a region contains three non-equivalent wells. A deep reactant well is connected to a symmetric double-well corresponding to two rotational conformers P and P' (see Fig. 1). The transfer from the reactant well to the double P and P' basin is well described by two active coordinates $\theta \in [0, \pi]$ and $\phi \in [-\pi, \pi]$ which are the spherical angles of the migrating atom H with respect to the center of the CO bond. This three-well region is an interesting pinball topography which suggests different control processes. The Hamiltonian is given

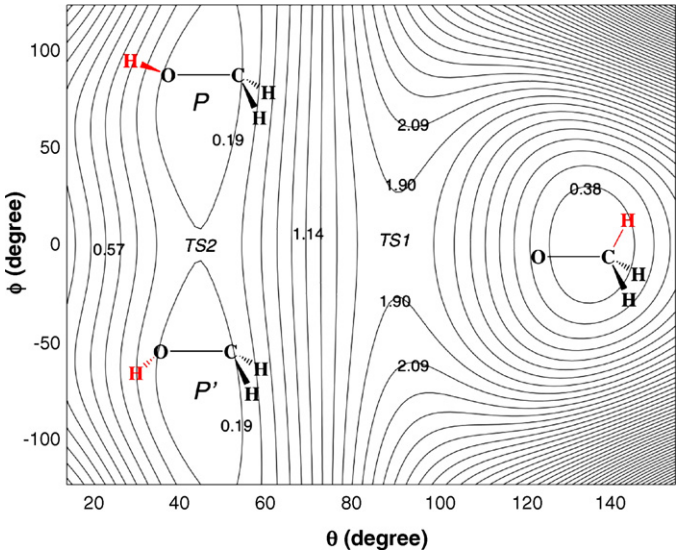

Fig. 1. Isoenergy contours (in eV) in the model potential energy surface of the isomerization $H_3CO \rightarrow H_2COH$ as a function of two active angular coordinates. The zero of energy is at the bottom of the product well (P or P'); the energies of the reactive well and of the transition states, *TS1* and *TS2*, are respectively: 0.181 eV, 1.854 eV, 0.195 eV.

by

$$\hat{H}^{2D} = -\frac{\hbar^2}{2I_\theta}\left(\frac{\partial^2}{\partial\theta^2} + \operatorname{cotan}\theta\frac{\partial}{\partial\theta}\right) - \frac{\hbar^2}{2I_\phi}\frac{1}{\sin^2\theta}\frac{\partial^2}{\partial\phi^2} + V(\theta,\phi) \quad (15)$$

where Euclidian normalization convention is adopted. The inertia moments are $I_\theta = 6160$ au and $I_\phi = 4430$ au. The model potential is calibrated on an *ab initio* computation at the QCISD level [58]. Analytical expressions of the potential and of the dipolar momentum surfaces are given respectively in Refs. [58] and [31]. In the C_S geometry ($\phi = 0$), the barrier height at the first transition state *TS1* from the reactant is 1.673 eV (13494 cm^{-1}). The barrier for the internal rotation at *TS2* is 0.195 eV (1573 cm^{-1}).

We focus on the symmetric double well region. In this example, we consider the first two delocalized states in the double well. The vibrational quantum number for the θ oscillator remains equal to zero. The states of parity even and odd should be denoted as $|0_+,0\rangle$ and $|0_-,0\rangle$ but, they will be simply written as $|0_+\rangle$ and $|0_-\rangle$. The splitting of the first level $|0_+\rangle - |0_-\rangle$ is 4.3×10^{-5} eV (0.35 cm^{-1}). This corresponds to a rather long tunneling time of about 48 ps much longer than the duration of the pulses used in the control. The target of the control is the localization of the ground delocalized state, $|0_+\rangle$, into one of the well P or P' (see Fig. 1) which corresponds to a localized wave function $|L\rangle$ or $|R\rangle$:

$$|L\rangle = \frac{|0_+\rangle + |0_-\rangle}{\sqrt{2}} \qquad |R\rangle = \frac{|0_+\rangle - |0_-\rangle}{\sqrt{2}}. \quad (16)$$

The goal is thus the creation of a superposed state and therefore of a coherence between the two levels. We adopt a coupling function (Eq. (5)) of the form $f(\mathbf{q}) = \cos(\phi) + \sin(\phi)$. The molecule is assumed to be aligned in the laboratory axis frame. $\vec{e}_z$ is directed along the CO axis. We use two polarization directions $\vec{e}_x$ and $\vec{e}_y$. The corresponding dipolar functions $\mu_x(\theta,\phi)$ and $\mu_y(\theta,\phi)$ are symmetrical and antisymmetrical functions, respectively.

4. STIRAP and Markovian dissipation

The control strategy which is used in this section is based on Stimulated Raman Adiabatic Passage or extension of this technique such as f-STIRAP (see [44,45] and references therein for a complete overview). STIRAP is a process involving a counterintuitive sequence of two pulses in a three-level system in which the field of the Stokes pulse precedes and overlaps the field of the pump pulse. The f-STIRAP strategy differs from the Stirap one by the fact that the pump and the Stokes pulses have the same amplitude at the end of the field. The idea which is at the basis of most of adiabatic schemes is to follow an adiabatic state corresponding respectively to the initial state when the field is switched on and to the target state when it is switched off. Such techniques are particularly efficient to achieve population transfer but can also be used to implement quantum gates [31]. Some investigations have already been performed in dissipative quantum systems [46–49]. All these studies have pointed out the negative effect of dissipation on the efficiency of STIRAP techniques.

In this section, we consider the 2D model and the influence of a Markovian dissipative bath upon the controlled dynamics by f-STIRAP. We limit our study to the Markovian dynamics in order to discuss the control properties from a numerical and analytical point of view. Indeed, the simple form of Markovian master equations allows the derivation of analytical formulas. The technical aspects of the analytical calculations are reported in Appendix A. The behaviour of the control under non-Markovian dissipation is expected to be similar but is not treated in this paper.

We now analyse the processes $|0_+\rangle \to |L\rangle$ and $|0_+\rangle \to |R\rangle$ which will allow us to detail the different steps of the control strategy (see also Ref. [31] for a complete description). Other control schemes can be analysed with the same kind of arguments. We first select an adiabatic technique adapted to the structure of the energy levels and to the dipolar matrix elements. We consider for that purpose the three levels $|0_+\rangle$, $|0_-\rangle$ and $|2_+\rangle$. Other set of levels could be selected. Taking into account the particular symmetry of the dipole moment in this basis, we choose the f-STIRAP strategy. To be more precise, we recall for instance that μ_x only couples the levels $|0_+\rangle$ and $|2_+\rangle$, the transition $|0_-\rangle$ to $|2_+\rangle$ being forbidden. The f-STIRAP strategy differs from the Stirap one by the fact that the pump and the Stokes pulses have the same amplitude at the end of the field. We assume that the two pulses are Gaussian with the frequency $\omega = E_{2_+} - (1/2)(E_{0_+} + E_{0_-})$ and that the Rabi frequencies are the same for the two pulses. The scheme can be summarized as follows

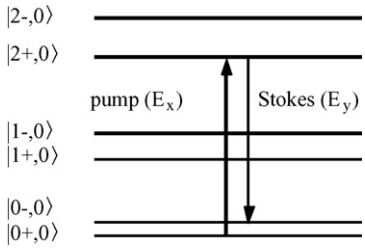

where the Stokes pulse is polarized along the $\vec{e}_y$ direction and the pump pulse along the $\vec{e}_x$ one. Simple algebra shows that the adiabatic state which has to be considered here can be written in the following form

$$|\psi_0(t)\rangle = \frac{1}{\sqrt{\Omega_x^2 + \Omega_y^2}}(\Omega_y|0_+\rangle - \Omega_x|0_-\rangle), \quad (17)$$

the two Rabi frequencies fulfilling the conditions

$$\lim_{t\to-\infty}\frac{\Omega_x}{\Omega_y} = 0 \quad \text{and} \quad \lim_{t\to+\infty}\frac{\Omega_x}{\Omega_y} = \pm 1 \quad (18)$$

where $\Omega_x = |\mu_x^{(0+/2+)}E_x|$ and $\Omega_y = |\mu_y^{(0-/2+)}E_y|$. One then deduces that $|\psi_0(-\infty)\rangle = 0_+\rangle$ and $|\psi_0(+\infty)\rangle = (1/\sqrt{2})[|0_+\rangle \mp |0_-\rangle]$ which corresponds to a perfect transfer in the adiabatic limit. However, this adiabatic limit requires pulses of very long duration. A standard condition is for instance $\Omega t_f \gg 1$

where Ω is the peak Rabi frequency and t_f the duration of the pulse.

It is clear that this long duration is not compatible with dissipation since the control cannot cancel the effect of dissipation. A precise mathematical description of this point is given by the notion of controllability [59,60] but goes beyond the scope of this paper. One therefore concludes that the target state cannot be reached exactly in the dissipative case even in the adiabatic limit. The idea is then to reduce the duration of the overall field. In order to keep the efficiency of the control as high as possible, we consider the adiabatic pulse as a laser field depending on several parameters (Rabi frequencies, delay between the pulses) and we optimize these parameters for a given duration. The optimization has been done on a grid to preserve as much as possible the robustness of the process.

Figs. 2 and 3 illustrate the results of applying the f-STIRAP strategy. Very good localization is obtained for a parameter λ lower than 1×10^{-3}, this localization decreasing smoothly as λ increases. The localization is close to 0.99 is the non-dissipative case [31]. The total duration of the process is here a crucial

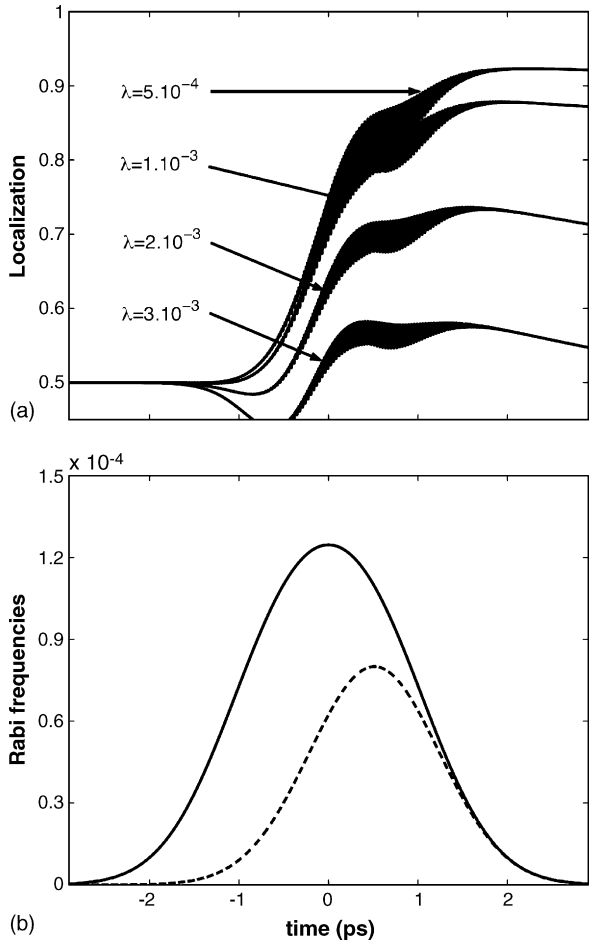

Fig. 2. Dynamics controlled by f-STIRAP strategy for the preparation of the superposed state $|R\rangle$. Panels (a) and (b) show, respectively, the evolution of the localization in the right well for different values of λ and the Rabi frequencies of the different pulses. Rabi frequencies are in atomic units. The solid line of panel (b) corresponds to the Stokes pulse and the dashed one to the pump pulse. The total duration of the process is of the order of 4.5 ps.

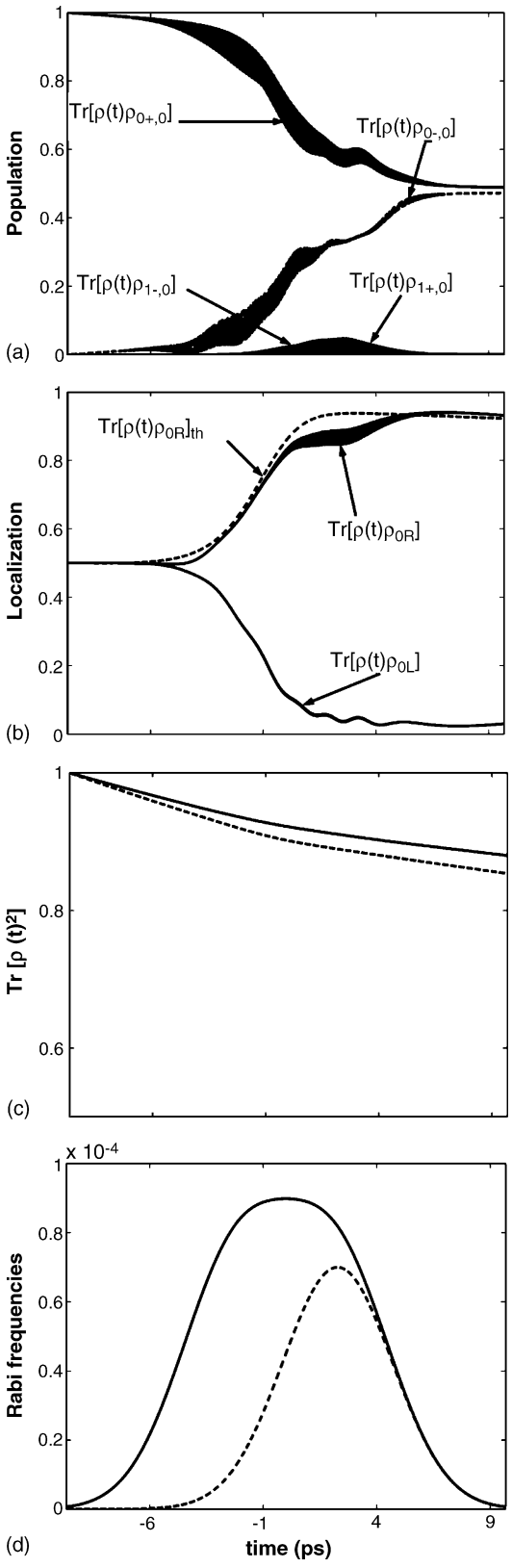

Fig. 3. Same as Fig. 2. Panels (a) and (b) represent the evolution of populations in the Hamiltonian eigenbasis and in the superposed states $|L\rangle$ and $|R\rangle$. Populations of other vibrational states remain small during the process. The dashed lines of panels (b) and (c) depict the results of analytical calculations (see text). The total duration of the pulse is of the order of 20 ps.

parameter and must be of the same order of the typical decay time induced by the dissipation. This latter time is proportional to $1/\lambda^2$.

Fig. 3 shows the excellent agreement between analytical and numerical calculations for the description of the evolution of $\mathrm{tr}[\rho^2]$ (panel (c)) and of $\mathrm{tr}[\rho(t)\rho_R]$ (panel (b)). Using equations of Appendix A, it can be shown that

$$\mathrm{tr}[\rho(t)\rho_L] = \frac{1}{4} - \frac{\Omega_x\Omega_y}{\Omega^2} + \left(\frac{1}{2} + 3\frac{\Omega_x\Omega_y}{\Omega^2}\right)\rho_{00}(t) \tag{19}$$

where $\rho_{00}(t)$ is given by Eq. (A12). The analysis of Eq. (19) shows that the localization roughly decreases exponentially with λ and the duration of the process. In the case where the two Rabi frequencies have the same maximum and the same shape, one sees that the localization is independent of this maximum. In the regime described by the analytical calculations, an increase of the Rabi frequencies does not improve the efficiency of the control.

The robustness of the strategies has been checked against two parameters, the time delay between successive pulses and the peak Rabi frequency, and for two different values of λ. This point is shown in Fig. 4. In each case, a satisfactory robustness is achieved around the maximum of localization. This maximum decreases with the dissipation but the range of robustness seems not affected. We also notice a shifting of the white region towards smaller delays as λ increases whereas this region does not move along the vertical axis. This confirms the idea that an efficient strategy consists in reaching as quickly as possible the target state in order to avoid the negative effect of dissipation. As mentioned above, this point is also justified by the analytical calculations.

5. Optimal control

We compare the role of the coupling with a discrete or continuous ensemble of oscillators. In the first case, OCT is applied in the total Hilbert space (system + bath) by propagating the wave packet with the coupled harmonic adiabatic channels. The coupled bath modes are thus exactly taken into account. The continuous case is treated in Liouville space with a Markovian or non-Markovian master equation. We first summarize the technical points of the implementation of OCT in both cases and we next gather the results.

5.1. OCT with coupled harmonic adiabatic channels

Different monotonically convergent algorithms for solving optimal control problems in the Hilbert space have been proposed. The objective functional can be defined in different manners [61,62] which are strongly connected [63]. We choose the functional which decouples the boundary conditions for the initial wave packet and the Lagrange multiplier [61] (functional called of type I in the recent analysis [63])

$$J = |\langle\psi_i(t_f)|\phi_f\rangle|^2 - \alpha\int_0^{t_f} E^2(t)\,\mathrm{d}t - 2\Re e\left[\int_0^{t_f}\langle\psi_i(t)|\psi_f(t)\rangle\langle\psi_f(t)|\partial_t - \hat{H}|\psi_i(t)\rangle\,\mathrm{d}t\right] \tag{20}$$

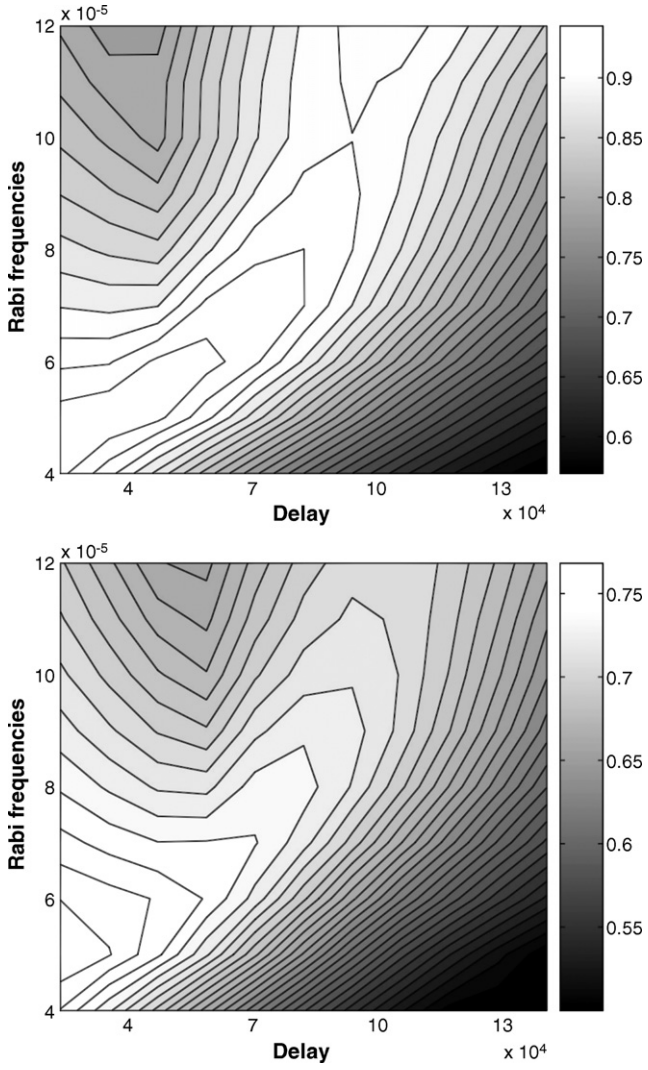

Fig. 4. Robustness of the f-STIRAP process as a function of the peak Rabi frequency and the delay between the pulses for a total duration of 4.5 ps of the overall field. Rabi frequency and delay are in atomic units. The upper and the lower part of the figure correspond, respectively, to $\lambda = 5\times10^{-4}$ and $\lambda = 2\times10^{-3}$.

The objective yield is measured by $O(t_f) = |\langle\psi_i(t_f)|\phi_f\rangle|^2$. The procedure to maximize the cost functional under constraint is described in details in the literature [64]. One obtains three coupled equations: the Schrödinger equation for $|\psi(t)\rangle$ with an initial condition $|\psi_i(t=0) = |\phi_i\rangle$ (forward propagation), the Schrödinger equation for the Lagrange multiplier $|\psi_f(t)\rangle$ with a final target condition $|\psi_f(t_f)\rangle = |\phi_f\rangle$ (backward propagation) and an equation for each component of the optimal field (here $E_x(t)$ and $E_y(t)$)

$$E_j(t) = -\left(\frac{1}{\hbar\alpha}\right)\Im m[\langle\psi_i(t)|\psi_f(t)\rangle\langle\psi_f(t)|\mu_j|\psi_i(t)\rangle] \tag{21}$$

where α is a positive penalty factor which weights the influence of the laser fluence. An experimental switching function $s(t) = \sin^2(\pi t/t_f)$ is usually introduced [64], α is then replaced by $\alpha \to \alpha/s(t)$. The equations are solved by an iterative formulation [61] and we use the improvement proposed in Ref. [65].

At each iteration, the field is given by $E_j^{(k)} = E_j^{(k-1)} + \Delta E_j^{(k)}$ where $\Delta E_j^{(k)}$ is calculated by Eq. (21).

The propagation is carried out by the closed coupled equations in the adiabatic basis set, which is in this case a harmonic basis set. Indeed, the separation between the active coordinates, $\mathbf{q} = [\theta, \phi]$, and the bath modes, $\mathbf{Q} = [Q_1, \ldots, Q_{\mathrm{Nb}}]$, leads naturally to an adiabatic separation [66–75] of the basis set into an active part, $\varphi_I(\mathbf{q})$, and a bath one, $\chi_U(\mathbf{Q};\mathbf{q})$. Therefore, the time-dependent wave function can be expressed as follows:

$$\Psi(\mathbf{q}, \mathbf{Q}, t) = \sum_{I,U} C_{I,U}(t) \times \varphi_I(\mathbf{q}) \times \chi_U(\mathbf{Q}; \mathbf{q})$$

The $\chi_U(\mathbf{Q};\mathbf{q})$ basis functions depend parametrically on the active coordinates and they can be viewed as adiabatic channels along the active coordinates. They are also the eigenfunctions of the N_b-Harmonic Hamiltonian, $\sum_j^{N_b}[((\hat{P}_j^2/2) + ((1/2)\omega_j^2))(Q_j - (c_j f(\mathbf{q})/\omega_j^2))]$. Thus, the $\chi_U(\mathbf{Q};\mathbf{q})$ basis functions are simply the product of N_b 1D-Harmonic eigenfunctions and are labeled by means of the excitations in the N_b bath normal modes, j_U. Those retained go from the ground state onwards to some maximal excitations, $\mathrm{Max}_{\mathrm{excit}}$ or more precisely, $\sum_j^{N_b} j_U \leq \mathrm{Max}_{\mathrm{excit}}$. The values of c_j are obtained using Eq. (8) (see Ref. [35]) where the frequency ω_m is the largest value among the N_b harmonic frequencies.

After integration over the bath modes, the total Hamiltonian can be rewritten as a matrix in (U,V) of operators acting only on the active variables, $\hat{\mathbf{H}}_{\mathrm{UV}}^{\mathrm{eff}}(\mathbf{q}, \partial_{\mathbf{q}})$ or as a set of coupled effective Hamiltonians. This representation is strictly equivalent to the initial Hamiltonian (Eq. (1)), provided the bath basis set is complete [58,74]. Since the coupling between the active coordinates and the bath modes is present only in the potential, the general expressions of the effective operators are simplified as follows:

$$\hat{\mathbf{H}}_{\mathrm{UV}}^{\mathrm{eff}}(\mathbf{q}, \partial_{\mathbf{q}}) = \hat{H}_0^{\mathrm{ND}} \delta_{\mathrm{UV}} + \sum_{i=1}^{\mathrm{ND}} f_{1,\mathrm{UV}}^{i}(\mathbf{q}) \partial_i + \Delta V_{\mathrm{UV}}^{\mathrm{eff}}(\mathbf{q}) \qquad (22)$$

Furthermore, the main contribution of the diagonal value of the $\Delta V_{\mathrm{UV}}^{\mathrm{eff}}(\mathbf{q})$ matrix is mainly the harmonic energy of the N_b-harmonic oscillators. The diagonal correction, the off-diagonal term of $\Delta V_{\mathrm{UV}}^{\mathrm{eff}}(\mathbf{q})$ and $f_{1,\mathrm{UV}}^{i}(\boldsymbol{q})$ matrices are due to the kinetic contribution associated with the active coordinates of the adiabatic basis functions.

In the present study, the choice of the initial, $|\phi_i\rangle$, and the target, $|\phi_f\rangle$, wave packets is fundamental fundamental in order to compare the results with Markonvian and non-Markovian propagation. Indeed, for the last two propagation schemes, the initial and the target wave packets are built with the spectral basis-set of $\hat{H}_0^{\mathrm{ND}}$ without bath contribution. $|\phi_i\rangle$ is the ground state, $|0_+\rangle$ and $|\phi_f\rangle$ is the sum of the ground state and the first excited state, $(1/\sqrt{2})(|0_+\rangle + |0_-\rangle)$. For the coupled adiabatic channels, we have chosen the same wave packets for the active contribution and the ground state of the harmonic bath basis function, $|\chi_0\rangle$ $(U=0)$:

$$|\phi_i\rangle = |0_+\rangle|\chi_0\rangle \qquad |\phi_f\rangle = \frac{1}{\sqrt{2}}(|0_+\rangle + |0_-\rangle)|\chi_0\rangle$$

The propagation of the wave packets has been obtained through the Taylor expansion of the evolution operator [76,77] with an order (here fifth order), which ensures the time reversibility and norm conservation of wave packet.

The primary basis sets are the normalized spherical harmonics and the number of spectral basis functions of $\hat{H}_0^{\mathrm{ND}}$ is 30. All the integrals are performed numerically with the help of a Gaussian quadrature scheme adapted to the basis. The integrals and the propagations have been performed with the *ElVibRot* program [78,74].

The number of bath modes, N_b, used here is 5. This method is also named *2 + 5D*. The values of ω_j are equal to: 133.3, 266.6, 400, 533.3, 666.6 cm^{-1}. Note that the value of the parameter $\mathrm{Max}_{\mathrm{excit}}$ is large enough to ensure the convergence of the propagation with the optimal electric field. The variation of the objective of quantum control is around 0.1 or 0.2% when $\mathrm{Max}_{\mathrm{excit}}$ increases by one. Moreover, $\mathrm{Max}_{\mathrm{excit}}$ depends on the coupling, c_j or more precisely on λ. The optimal values of $\mathrm{Max}_{\mathrm{excit}}$ are, respectively, 2 and 3 for a parameter λ equal to 5×10^{-4} and 2×10^{-3}. With the *N + 5D* model, the number of harmonic adiabatic channels are, respectively 21 and 56 when $\mathrm{Max}_{\mathrm{excit}} = 2$ or 3.

5.2. OCT with Markovian and non-Markovian dissipation

We use the density matrix approach suited to include coupling with a bath. Different approaches have been proposed [79,80]. We adopt here a monotonically convergent algorithms adapted for the Liouville space [40,63]. The objective is the maximization of $O(t_f) = |\langle\langle W^\dagger|\rho(t_f)\rangle\rangle|^2$ where W is the target operator. (A different choice which minimizes the discrepancy Tr (D^2) where $D = \rho(t_f) - W$ has been recently suggested for dissipative systems [81].) According to our procedure in Hilbert space, we adopt the functional which decouples the boundary conditions [63]. The optimization procedure of the chosen functional leads to coupled equations of motion for the density matrix $|\rho(t)\rangle\rangle$ (in superoperator notation), the Lagrange multiplier $|\Xi(t)\rangle\rangle$ (which imposes that the Liouville equation remains fulfilled at any time) and the laser field $E(t)$. $|\rho(t)\rangle\rangle$ is propagated forwards with an initial condition while $|\Xi(t)\rangle\rangle$ is propagated backwards with a final condition. In this formulation, each component of the field is given by

$$E_j(t) = \frac{-\Im m\{\langle\langle\rho(t)|\Xi(t)\rangle\rangle\langle\langle\Xi(t)|M_j|\rho(t)\rangle\rangle\}}{\alpha} \qquad (23)$$

where $\langle\langle A^\dagger|B\rangle\rangle = \mathrm{Tr}(AB)$, $M_j|\rho(t)\rangle\rangle = |\mu_j\rho(t)\rangle\rangle - |\rho(t)\mu_j\rangle\rangle$ and α is the penalty factor, including the $s(t)$ function. The field is built iteratively by a convergent algorithm [40] adapted to non-Markovian dissipation [39]. If we design by $\Gamma(t)$ the memory kernel given by Eqs. (10) and (11), the forward propagation with an initial condition and the backward propagation with a final

condition satisfy the following equations

$$\frac{\partial}{\partial t}||\rho(t)\rangle\rangle = -\frac{i}{\hbar}\left[L_0^{\mathrm{nD}} - \sum_j M_j E_j(t)\right]||\rho(t)\rangle\rangle - \int_0^t \mathrm{d}\tau\, \Gamma(t-\tau)||\rho(\tau)\rangle\rangle \quad (24)$$

$$\frac{\partial}{\partial t}||\Xi(t)\rangle\rangle = -\frac{i}{\hbar}\left[L_0^{\mathrm{nD}} - \sum_j M_j E_j(t)\right]||\Xi(t)\rangle\rangle + \int_t^{t_f} \mathrm{d}\tau\, \Gamma(\tau-t)||\Xi(\tau)\rangle\rangle \quad (25)$$

where $L_0^{\mathrm{nD}}|\rho(t)\rangle\rangle = |\hat{H}_0^{\mathrm{nD}}\rho(t)\rangle\rangle - |\rho(t)\hat{H}_0^{\mathrm{nD}}\rangle\rangle$. The bath correlation function appearing in Eqs. (10) and (11) is computed by Eq. (12) for different frequencies ω_c and temperatures.

5.3. Results

In each example, the zero-order field is the one optimized without dissipation in the wave packet formalism. The objective yield was then 99.999%. This procedure is efficient for two main reasons. First, the OCT algorithm in presence of dissipation converges very fast for different baths and in most cases, the convergence is always achieved in about 20 iterations (see Table 2). Second, starting with the same zero-order field enforces the algorithm to converge towards the same type of solutions for the different strategies in the Hilbert (cHAC) or Liouville space. We recall that two polarizations and therefore two pulses $E_x(t)$ and $E_y(t)$ are used. The first one has a duration equal to $t_{f1} = 0.5$ ps. This is the shortest duration which avoids a too strong field, the limit being fixed at $|E_{\max}| = 0.05$ au (1 au = 5.14 10^9 V cm^{-1}). For the second pulse, we have $t_{f2} = 4.5$ ps which is the shortest time reached by STIRAP scheme. The two pulse durations must be compared with the characteristic time of the field free dynamics (we recall that the tunneling time is 48 ps and the typical decay time of the dissipation without field τ_R is of the order of $1/\lambda^2$, i.e. $\tau_R \approx 6$ ps for $\lambda = 2 \times 10^{-3}$). They must be also compared with the correlation time of bath to foresee the role of the memory effect (see Table 1). t_{f1} is of the order of magnitude of some correlation times so this corresponds to an intermediate memory case. $t_{f\,2}$ is larger than the correlation times, the situation is of short memory and Markovian dynamics is expected to be sufficient.

5.3.1. Short pulse

Table 2 gathers the objective yields obtained by cHAC, Markovian and non-Markovian dynamics with different baths for the first short pulse of duration t_{f1}. We give the objective yield with the zero-order field O(0) (the optimal field without dissipation) and after the first iteration O(1). This confirms the quality of the zero-order field. $O(itc)$ gives the final performance and the number itc of required iterations. One observes that for the weak coupling $\lambda = 5 \times 10^{-4}$ each method converges easily because the performance index is already very high with the zero-order field. We focus now on the case with a coupling $\lambda = 2 \times 10^{-3}$ which is the maximum value ensuring convergence of the cHAC method with the chosen basis set. cHAC with (2 + 5)D starts with the smallest yield but succeeds in reaching a good performance. Due to dissipation, both Markovian and non-Markovian dynamics do not reach the objective yield with 100% efficiency. As can be expected for the pulse in the intermediary memory case, the results are not the same for Markovian and non-Markovian dynamics but they remain of the same order of magnitude. Dissipation remains weak during the pulse duration t_{f1} but memory effects are not completely negligible mainly for $\omega_c = 100$ cm^{-1}. In that case, $\tau_{1/2} = 50$ fs and $\tau_{\max} = 500$ fs which is of the order of $t_{f1} = 500$ fs.

We now give some details for the case with $\lambda = 2 \times 10^{-3}$, $\omega_c = 400$ cm^{-1}, $T = 298$ K and t_{f1}. Fig. 5 show the two components $E_x(t)$ and $E_y(t)$ of the optimal field obtained by cHAC, Markov and non-Markovian dissipation.

The zero order $E_x(t)$ field is very simple and mainly formed by a half cycle pulse with a shape corresponding to the $s(t)$ function. The transfer of population is realized by the short half pulse of the $E_y(t)$ component [31]. The action of the $E_x(t)$ field roughly corresponds to a Stark effect. At the maximum of the pulse, the laser field adds an effective potential which strongly decreases the barrier of the energy landscape. In this example, the barrier height is pulled down of about 75%. One observes that the fields keep the same shape when dissipation occurs. A manifestation of the memory effect can be seen in the pulse duration t_{f1} but the discrepancy remains very small between Markovian and non-Markovian dynamics.

Fig. 6 give the evolution of the population in the $|0_+\rangle$and $|0_-\rangle$ states and the absolute value of the coherence $|\rho_{0_+,0_-}(t)|$

Table 2
Objective yield $O(itc) = |\langle\langle W^\dagger|\rho_{itc}(t_f)\rangle\rangle|^2$ after different iterations for the short pulse $t_{f1} = 500$ fs

	T (K)/λ/ω_c (cm^{-1})									
	298/5 × 10^{-4}/400			298/2 × 10^{-3}/400			100/2 × 10^{-3}/400		298/2 × 10^{-3}/100	
	2 + 5D[a]	Mar[a]	N.Mar[a]	2 + 5D[a]	Mar[a]	N.Mar[a]	Mar[a]	N.Mar[a]	Mar[a]	N.Mar[a]
$O(0)$ %	98.4	99.4	99.4	90.7	94.5	94.3	97.6	96.9	82.8	89.7
$O(1)$ %	99.1	99.6	99.6	96.5	94.7	94.6	97.8	97.2	83.0	90.1
$O(itc)$ %	99.6	99.6	99.6	97.9	94.7	95.3	97.8	97.3	83.1	94.4
itc	20	20	20	20	20	20	20	20	20	20

λ is the system-bath coupling and ω_c is the reference frequency of the Ohmic spectral function (Eq. (7)).
[a] Model.

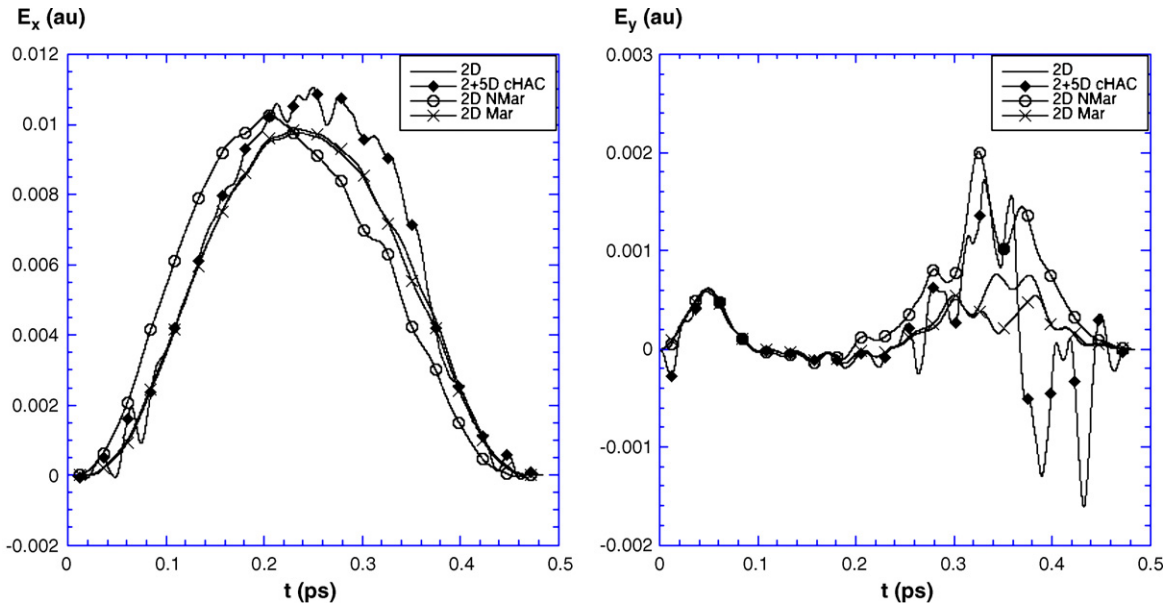

Fig. 5. OCT field $E_x(t)$ and $E_y(t)$ for the 2D case with $\lambda = 2 \times 10^{-3}$, $\omega_c = 400\,\mathrm{cm}^{-1}$, $T = 298$ K. We compare cHAC, Markovian and non-Markovian dynamics.

of the superposed state. As can be expected, the coherence is more sensitive to the dissipation effect than the populations, particularly in the non-Markovian case. Note that, after t_{f1}, the dynamics corresponds to a field-free dynamics.

The analysis of the dissipation helps to understand the difficulty to reach the highest yield. Indeed, the OCT procedure has to optimize two processes: (i) Maximization of the localization of the wave packet or the density matrix; (ii) Minimization of the effect of dissipation of the system through the bath modes. The first process is relatively easy to reach with our 2D-model, as it has been shown previously [31]. However, it might be more difficult to fight against the dissipation effect. The following figures (Figs. 7 and 8) illustrate this point by comparing the field-free dynamics and the dynamics with the optimal field. The parameter, $\mathrm{Tr}[\rho^2(t)]$, is used for the Markovian and non-Markovian dynamics while the population on the first channel or the partial trace of ρ over the first channel, $\mathrm{Tr}[\rho_{\mathrm{ch}_1}]$, is used for cHAC dynamics.

For the Markovian and the non-Markovian cases, the field-free dynamics shows a large diminution of $\mathrm{Tr}[\rho^2(t)]$ when the time increases (see Fig. 7), in particular for the strong dissipation case ($\lambda = 2 \times 10^{-3}$, $\omega_c = 100\,\mathrm{cm}^{-1}$ and $T = 298$ K, Fig. 7b). However, this diminution is smaller for the dissipative dynamics with optimal field, which illustrates how the optimal field fights dissipation to get the highest objective yield. Furthermore, in the case of the non-Markovian dynamics with the optimal field, the

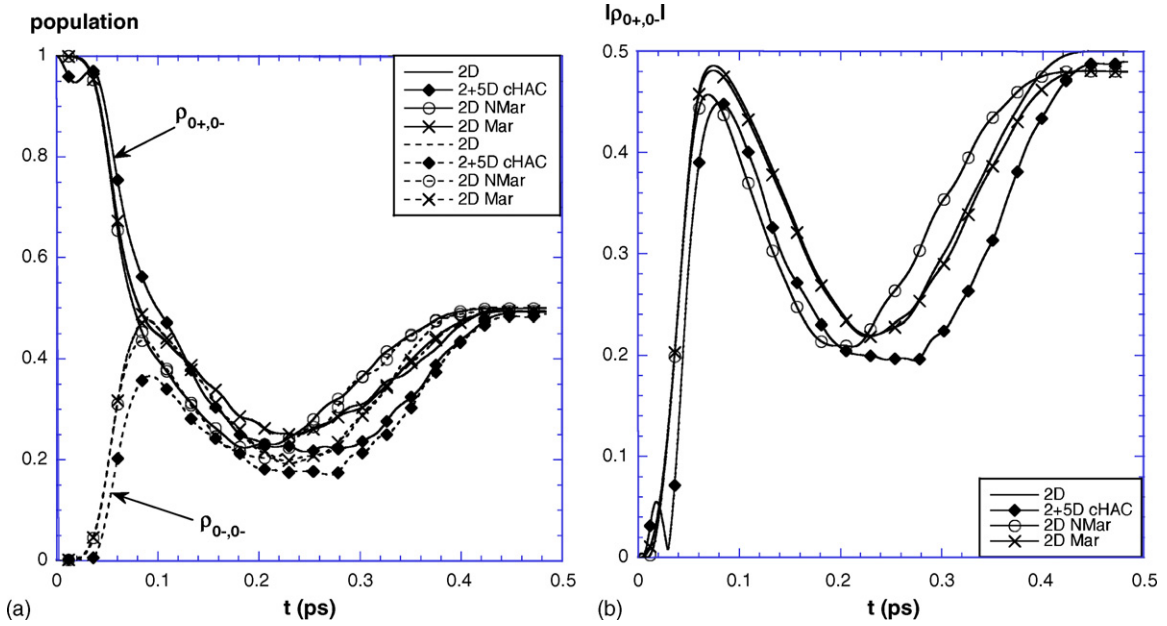

Fig. 6. Evolution of the population $\rho_{0_+,0_+}(t)$ and $\rho_{0_-,0_-}(t)$ (panel a) and of the coherence $|\rho_{0_+,0_-}(t)|$ (panel b) for the 2D case with $\lambda = 2 \times 10^{-3}$, $\omega_c = 400\,\mathrm{cm}^{-1}$, $T = 298$ K (see Fig. 5).

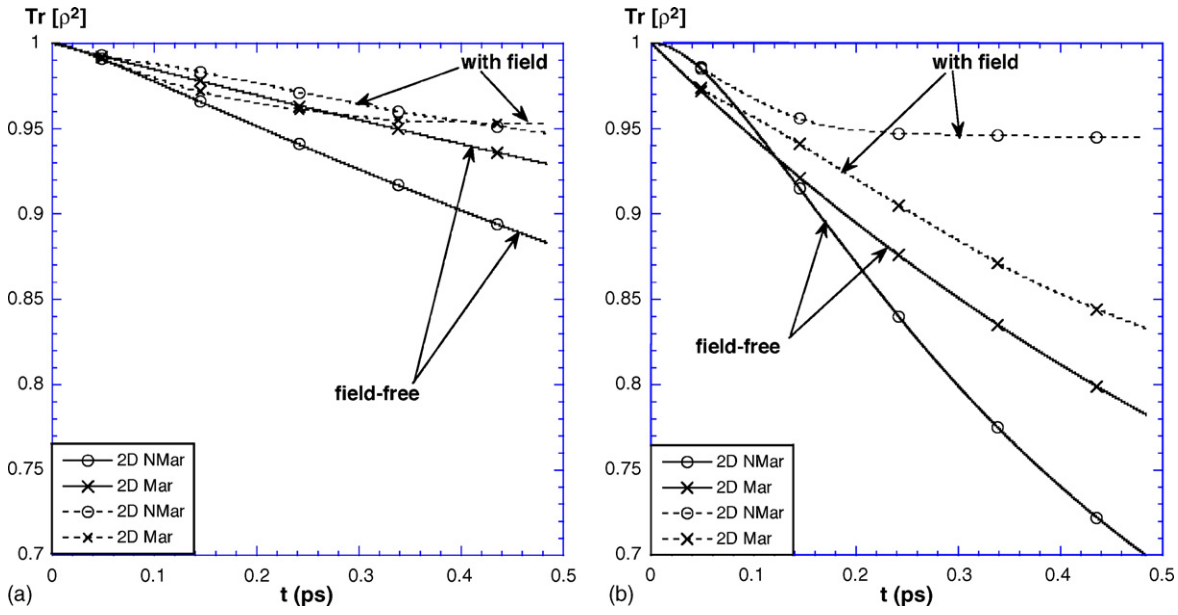

Fig. 7. Evolution of the $\mathrm{Tr}[\rho^2(t)]$ for field-free dynamics (full line) and for a dynamics with the optimal field (dashed line), (panel a) with $\lambda = 2 \times 10^{-3}$, $\omega_c = 400\,\mathrm{cm}^{-1}$, $T = 298$ K; (panel b) for the 2D case with $\lambda = 2 \times 10^{-3}$, $\omega_c = 100\,\mathrm{cm}^{-1}$, $T = 298$ K.

diminution of $\mathrm{Tr}[\rho^2(t)]$ is much smaller than in the case of the Markovian one. The necessity of taking into account memory effect is obvious in that case.

We note that the final value of $\mathrm{Tr}(\rho^2)$ is always nearly equal to the value of the objective yield, $[\mathrm{Tr}(W\rho)]^2$ (see Table 2). At convergence, $\mathrm{Tr}(D^2) \approx 0$ where $D = \rho - W$, so one has $\mathrm{Tr}(\rho^2) \approx -[\mathrm{Tr}(W^2) - 2\mathrm{Tr}(W\rho)]$ which can be recast as $\mathrm{Tr}(\rho^2) \approx -[1 - \mathrm{Tr}(W\rho)]^2 + [\mathrm{Tr}(W\rho)]^2$. Since $[1 - \mathrm{Tr}(W\rho)]^2$ can be neglected if ρ is close to W, one obtains $\mathrm{Tr}(\rho^2) \approx O_{t_f} = [\mathrm{Tr}(W\rho)]^2$.

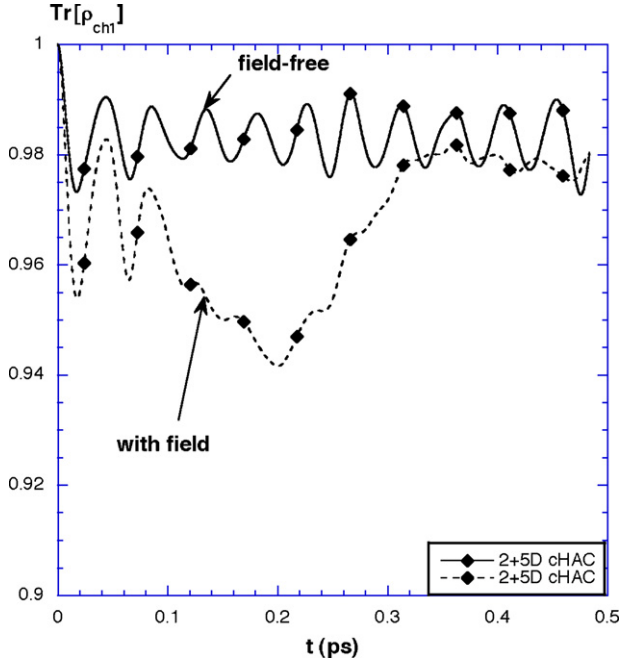

Fig. 8. Evolution of the population on the first channel, $\mathrm{Tr}[\rho_{\mathrm{ch}_1}]$, for field-free dynamics (full line) and for dynamics with the optimal field (dashed line), with $\lambda = 2 \times 10^{-3}$, $\omega_c = 400\,\mathrm{cm}^{-1}$.

In the case of the cHAC dynamics, the evolution of $\mathrm{Tr}[\rho_{\mathrm{ch}_1}]$ is different. Indeed, the number of bath modes seems insufficient to produce a strong dissipation. For the field-free dynamics, the evolution of $\mathrm{Tr}[\rho_{\mathrm{ch}_1}]$ presents some oscillations with a time scale equal to 0.05 ps and the average value is around 0.98. For the dynamics with the optimal field, the evolution of $\mathrm{Tr}[\rho_{\mathrm{ch}_1}]$ decreases and next increases to reach 0.98 which is close to the objective yield (see Table 2).

5.3.2. Long pulse

Table 3 is devoted to the long pulse case (t_{f2}). These results may be compared with the STIRAP approach (see Fig. 2).

The cHAC remains very efficient for a long time. Although the objective yield with the zero-order field is small (around 20%), the convergence is achieved very quickly. Indeed, in one iteration only, the yield increases up to 97%. On the contrary, OCT does not achieve high performance and the results are of the same order of magnitude than those obtained with STIRAP. Furthermore, the optimization process has almost no effect on the objective yield. In particular for the Markovian model, the

Table 3
Objective yield $O(itc) = |\langle\langle W^\dagger | \rho_{itc}(t_f)\rangle\rangle|^2$ after different iterations for the long pulse $t_{f2} = 4.5$ ps

	T (K)/λ/ω_c (cm^{-1})				
	$298/2 \times 10^{-3}/400$			$100/2 \times 10^{-3}/400$	
	2 + 5D[a]	Mar[a]	N.Mar[a]	Mar[a]	N.Mar[a]
$O(0)$ %	20.7	68.1	57.5	85.2	79.4
$O(1)$ %	97.4	68.1	58.9	85.2	80.2
$O(itc)$ %	99.4	68.2	67.7	85.3	81.6
itc	10	20	20	20	20

λ is the system-bath coupling and ω_c is the reference frequency of the Ohmic spectral function (Eq. (7)).
[a] Model.

Table 4
Objective yield $O(itc) = |\langle\langle W^{\dagger}|\rho_{itc}(t_f)\rangle\rangle|^2$ for the Hadamard gate after different iterations for the short pulse $t_{f1} = 0.5$ ps

	T (K)/λ/ω_c (cm^{-1})				
	298/5 × 10^{-4}/400			298/2 × 10^{-3}/400	
	2 + 5D[a]	Mar[a]	N.Mar[a]	Mar[a]	N.Mar[a]
$O(0)$ %	93.9	99.6	99.6	94.7	93.7
$O(1)$ %	95.3	99.6	99.6	94.7	93.8
$O(itc)$ %	98.5	99.6	99.6	94.7	94.3
itc	20	20	20	20	20

λ is the system-bath coupling and ω_c is the reference frequency of the Ohmic spectral function (Eq. (7)).
[a] Model.

increase of the yield is only of the order of 0.1%. Note that for the long pulse, the Markovian dynamics gives slightly a better objective yield than the non-Markovian one. It was the opposite for the short pulse (see Table 2).

5.3.3. Hadamard gate

Finally, we have applied OCT to generate the pulse able to realize the complete Hadamard transformation, $\hat{U}_{\mathrm{HAD}}$

$$\hat{U}_{\mathrm{HAD}} \begin{pmatrix} |0_+\rangle \\ |0_-\rangle \end{pmatrix} = \begin{pmatrix} \frac{1}{\sqrt{2}} \end{pmatrix} \begin{pmatrix} 1 & 1 \\ 1 & -1 \end{pmatrix} \begin{pmatrix} |0_+\rangle \\ |0_-\rangle \end{pmatrix} = \begin{pmatrix} |L\rangle \\ |R\rangle \end{pmatrix}.$$

Starting from the fundamental state $|0_+\rangle$, the pulse localizes the wave packet in the left well $|L\rangle = (|0_+\rangle + |0_-\rangle)/\sqrt{2}$ while starting from the first excited state $|0_-\rangle$ the same pulse localizes it in the right well $|R\rangle = (|0_+\rangle - |0_-\rangle)/\sqrt{2}$. The zero order field is the one optimized for one transformation with a pulse duration t_{f1} (see Section 5.3.1) and this field is almost optimal for the Hadamard gate, since the objective yield is always larger than 90% (see Table 4). For a weak dissipation ($\lambda = 5 \times 10^{-4}$, $\omega_c = 400\,\mathrm{cm}^{-1}$ and $T = 298$ K), the convergence is almost reached for all dissipative models (cHAC, Markovian and non-Markovian). For a strong dissipation ($\lambda = 2 \times 10^{-3}$, $\omega_c = 400\,\mathrm{cm}^{-1}$ and $T = 298$ K) the convergence is more difficult to reach and for the Markovian and non-Markovian models, the yield has not been improved after 20 iterations.

6. Concluding remarks

In a previous work, we have examined different characteristics of the laser control in a double or triple well topography without dissipation and we have shown the advantages and limits of STIRAP and OCT [31]. The adiabatic approach requires an intermediary states well decoupled from all the other ones. The 2D bifurcating surface (see Fig. 1) is a good example showing that some transitions from a well to another one cannot be controlled by STIRAP, for instance the passing from reactant (H_3CO) to P or P'. The delocalized states above TS1 are too strongly coupled by the dipolar momentum. OCT succeeds in realizing the localization but produces a very complicated pulse which may be unrealistic. On the contrary the symmetric P and P' double well offers many transfer pathways, which facilitates the obtaining of an optimal pulse both by STIRAP and OCT. In this case, the OCT method reaches a high performance with shorter laser pulses than STIRAP. These pulses are in addition very simple and realistic. One observes that the mechanism found by OCT mainly uses the Stark effect which modifies the profile of the potential energy surface. Dynamic Stark Control process has been recently suggested as a promising way to control reactivity with photonic reagents [82].

Here, we address the problem of the stability of these previous results against interaction with an environment. We have shown that even in quite difficult situations in which the environment is strongly coupled with the system (high temperature, low frequency of the bath and non-negligible coupling strength) laser control with short pulse duration succeeds in creating the coherence of the Hadamard gate with a good performance index (of the order of 95%). We have also found a pulse achieving to full Hadamard transformation with a similar result. The challenge will be now to implement other transformations and their concatenations.

Different comments about the laser control can be made. (i) STIRAP needs long pulses so the control must fight strongly against dissipation. Fig. 2 shows the difficulty to maintain an objective yield larger than 90% with increasing coupling. OCT allows to decrease the pulse duration and therefore to reach the objective with a high performance. (ii) OCT remains very efficient even for long pulses of the order of those used in STIRAP in the case of a discrete coupling to few oscillators. But this is in fact a laser control of a non-open 7D system treated partially with the harmonic approximation. The objective yield reaches 99.4% in 10 iterations and could be improved. On the contrary, the results obtained with Markovian or non-Markovian dynamics are in agreement with STIRAP results and are not so good. (iii) For a short pulse, memory effect plays a role. The non-Markovian approach predicts a more efficient fight against dissipation but however the discrepancy is not very important. Markovian and non-Markovian predictions merge when the reference frequency of the bath ω_c becomes larger than about $1000\,\mathrm{cm}^{-1}$. This frequency corresponds to a correlation time of about 3 fs, the memory effects are therefore negligible.

Finally, we can conclude that cHAC is a promising way to increase the number of degrees of freedom when the coupling with the bath is not too large. Furthermore, we point out that, the studies using adiabatic separation with two actives degrees of freedom are unusual. Some recent examples like logical gates on NH_3 [29] or other small molecules could be explored, mainly when potential energy surfaces exist. Worth noting, we have already developed a potential for ammonia for spectroscopic application and it is particularly well adapted to cHAC [74]. If no potential is available, cHAC permits easily a modelling with some oscillators and the results give more confidence in the success of laser control than the continuous dissipative model.

Acknowledgments

The computing facilities of IDRIS (Project numbers 061247 and 2006 0811429) as well the financial support of the FNRS in the University of Liège SGI Nic project are gratefully acknowledged.

Appendix A. Analytical estimations for an adiabatic control in a Markovian environment

In this appendix, we derive several analytical formulas, which allow to describe the dynamics of a system coupled to a Markovian bath and controlled by a f-STIRAP strategy. For that purpose, we follow and we generalize calculations of Ref. [51]. We denote by $|1\rangle$, $|2\rangle$ and $|3\rangle$ the three states involved in the control. To simplify the notations and to give them a general character, we write γ_{ij} the relaxation coefficient from the state $|i\rangle$ to the state $|j\rangle$ and $\tilde{\gamma}_i$ the sum $\sum_j \gamma_{ij}$. The level 3 is coupled resonantly respectively to the level 1 by the Rabi frequency Ω_x and to the level 2 by Ω_y (see Sec. 4). We work henceforth in the basis spanned by the states $|1\rangle$, $|2\rangle$ and $|3\rangle$.

After a RWA approximation, the Hamiltonian of the system can be written in representation interaction as

$$\begin{pmatrix} 0 & 0 & \Omega_x \\ 0 & 0 & \Omega_y \\ \Omega_x & \Omega_y & 0 \end{pmatrix} \tag{A1}$$

The adiabatic states $|\psi_0\rangle$, $|\psi_+\rangle$ and $|\psi_-\rangle$ are the eigenstates of the Hamiltonian with eigenvalues 0, Ω and $-\Omega$ where $\Omega = \sqrt{\Omega_x^2 + \Omega_y^2}$. Simple algebra leads to

$$\begin{cases} \psi_0 = \dfrac{1}{\Omega}(\Omega_y|1\rangle - \Omega_x|2\rangle) \\ \psi_+ = \dfrac{1}{\Omega\sqrt{2}}(\Omega_x|1\rangle + \Omega_y|2\rangle + \Omega|3\rangle) \\ \psi_- = \dfrac{1}{\Omega\sqrt{2}}(\Omega_x|1\rangle + \Omega_y|2\rangle - \Omega|3\rangle) \end{cases} \tag{A2}$$

We use the same adiabatic basis in the presence of dissipation. Introducing the density matrix ρ of the system and using Eq. (A2), the matrix elements of ρ in the adiabatic basis can be written as a function of the matrix elements of ρ in the diabatic basis. For instance we obtain that

$$\rho_{++} - \rho_{--} = \frac{1}{\Omega}[\Omega_x(\rho_{13} + \rho_{31}) + \Omega_y(\rho_{23} + \rho_{32})] \tag{A3}$$

where the notations can be deduced straightforwardly. Assuming that the relaxation terms are small as compared to the peak Rabi frequencies, it can be shown [31] that the off-diagonal terms ρ_{0_+}, ρ_{0_-} and ρ_{+-} of ρ in the adiabatic basis remains small and negligible. This assumption is made in order to simplify the analytical calculations and is checked numerically in Sec. 4. The next step consists in determining the diagonal elements ρ_{++}, ρ_{--} and ρ_{00} subject to the relation $\rho_{++} + \rho_{--} + \rho_{00} = 1$. Inverting Eq. (A2), one arrives to the following equations

$$\begin{cases} \rho_{13} + \rho_{31} = \dfrac{\Omega_x}{\Omega}(\rho_{++} - \rho_{--}) \\ \rho_{23} + \rho_{32} = \dfrac{\Omega_y}{\Omega}(\rho_{++} - \rho_{--}) \end{cases} \tag{A4}$$

As $(\partial\rho_{13}/\partial t) = -(1/2)(\tilde{\gamma}_1 + \tilde{\gamma}_3)\rho_{13} + \alpha_{13}$ and $(\partial\rho_{23}/\partial t) = -(1/2)(\tilde{\gamma}_2 + \tilde{\gamma}_3)\rho_{23} + \alpha_{23}$ where α_{13} and α_{23} correspond to the terms which do not depend on dissipation, we then have

$$\frac{\partial\rho_{++}}{\partial t} - \frac{\partial\rho_{--}}{\partial t} = \left[-\frac{\Omega_x^2}{2\Omega^2}(\tilde{\gamma}_1 + \tilde{\gamma}_3) - \frac{\Omega_y^2}{2\Omega^2}(\tilde{\gamma}_2 + \tilde{\gamma}_3)\right] \times (\rho_{++} - \rho_{--}) \tag{A5}$$

There is no contribution from the other terms as in the non-dissipative limit, ρ_{++} and ρ_{--} are constant in time. We assume initially, i.e. at $t \to -\infty$, that $\rho_{++}(-\infty) = \rho_{--}(-\infty) = 0$. We deduce from Eq. (A5) that $\rho_{++}(t) = \rho_{--}(t)$. To determine ρ_{00}, we use the fact that

$$\rho_{00} = \frac{1}{\Omega^2}(\Omega_y^2\rho_{11} + \Omega_x^2\rho_{22} - \Omega_x\Omega_y\rho_{12} - \Omega_x\Omega_y\rho_{21}) \tag{A6}$$

Deriving this expression with respect to the time and neglecting the derivatives of the Rabi frequencies which are assumed to be small, we obtain

$$\frac{\partial\rho_{00}}{\partial t} = \frac{1}{\Omega^2}\left(\Omega_y^2\frac{\partial\rho_{11}}{\partial t} + \Omega_x^2\frac{\partial\rho_{22}}{\partial t} - \Omega_x\Omega_y\frac{\partial\rho_{12}}{\partial t} - \Omega_x\Omega_y\frac{\partial\rho_{21}}{\partial t}\right) \tag{A7}$$

The next step consists in using the Schrödinger equation to replace the terms $\partial\rho_{11}/\partial t$, $\partial\rho_{22}/\partial t$, $\partial\rho_{12}/\partial t$ and $\partial\rho_{21}/\partial t$ by their expressions in terms of ρ_{11}, ρ_{22} and so on. We have, for instance, that

$$\frac{\partial\rho_{11}}{\partial t} = -\tilde{\gamma}_1\rho_{11} + \gamma_{12}\rho_{22} + \gamma_{13}\rho_{33} + \alpha_{11} \tag{A8}$$

Finally, we express these last terms as a function of ρ_{00}, ρ_{++} and ρ_{--} to derive the following equation:

$$\frac{\partial\rho_{00}}{\partial t} = \lambda(t) + \mu(t)\rho_{00} \tag{A9}$$

where

$$\lambda = \gamma_{12}\frac{\Omega_x^4 + \Omega_y^4}{4\Omega^4} + \gamma_{13}\frac{\Omega_y^4}{2\Omega^2} + \gamma_{23}\frac{\Omega_x^2}{2\Omega^2} \tag{A10}$$

and

$$\mu = -\frac{-\Omega_y^2}{\Omega^2}\tilde{\gamma}_1 - \frac{\Omega_x^2}{\Omega^2}\tilde{\gamma}_2 - \gamma_{13}\frac{\Omega_y^2}{2\Omega^2} - \gamma_{23}\frac{\Omega_x^2}{2\Omega^2} + \left[\frac{\Omega_x^2\Omega_y^2}{\Omega^4} - \frac{1}{2}\right]\gamma_{12} \tag{A11}$$

As $\rho_{00}(-\infty) = 1$, the solution of Eq. (A9) can be written as follows

$$\rho_{00}(t) = \int_{-\infty}^{t}\lambda(u)\,\mathrm{d}u + \exp\left[\int_{-\infty}^{t}\mu(u)\,\mathrm{d}u\right] \tag{A12}$$

References

[1] A. Igarashi, H. Yamada, Chem. Phys. 327 (2006) 395–405.
[2] H. Naundorf, K. Sudermann, O. Kühn, Chem. Phys. 240 (1999) 163–172.
[3] M.V. Korolkov, J. Manz, G.K. Paramonov, J. Chem. Phys. 100 (1996) 10874–10889.
[4] N. Došlić, O. Kühn, J. Manz, K. Sundermann, J. Phys. Chem. A 102 (1998) 9645–9650.

[5] N. Došlić, K. Sundermann, L. González, O. Mó, J. Giraud-Girard, O. Kühn, Phys. Chem. Chem. Phys. 1 (1999) 1249–1257.
[6] O. Kühn, Y. Zhao, F. Shuang, Y. Yan, J. Chem. Phys. 112 (2000) 6104–6112.
[7] O. Kühn, J. Phys. Chem. A 106 (2002) 7671–7679.
[8] H. Umeda, Y. Fujimura, Chem. Phys. 274 (2001) 231–241.
[9] H. Umeda, Y. Fujimura, J. Chem. Phys. 113 (2000) 3511–3518.
[10] H. Umeda, M. Takagi, S. Yamada, S. Koseki, Y. Fujimura, J. Am. Chem. Soc. 124 (2002) 9265–9271.
[11] D. Gerbasi, M. Shapiro, P. Brumer, J. Chem. Phys. 124 (2006) 074315.
[12] K. Hoki, Y. Ohtsuki, Y. Fujimura, J. Chem. Phys. 114 (2001) 1575–1581.
[13] Y. Fujimura, L. González, K. Hoki, J. Manz, Y. Ohtsuki, Chem. Phys. Lett. 306 (1999) 1–8.
[14] E. Geva, J. Chem. Phys. 116 (2002) 1629–1635.
[15] M. Artamonov, T.-S. Ho, H. Rabitz, J. Chem. Phys. 124 (2006) 064306.
[16] C. Uiberacker, W. Jakubetz, J. Chem. Phys. 120 (2004) 11532–11539, ibid 120 (2004) 11540–11548.
[17] V. Kurkal, S.A. Rice, Chem. Phys. Lett. 344 (2001) 125–137.
[18] H. Umeda, Y. Fujimura, J. Chem. Phys. 113 (2000) 3510–3518.
[19] J. Gong, A. Ma, S.A. Rice, J. Chem. Phys. 122 (2005) 144311, ibid 122 (2005) 204505.
[20] A. Kondorskiy, G. Mil'nikov, H. Nakamura, Phys. Rev. A 72 (2005) 041401.
[21] M. Artamonov, T.-S. Ho, H. Rabitz, Chem. Phys. 328 (2006) 147–155.
[22] C.M. Tesch, L. Kurtz, R. de Vivie-Riedle, Chem. Phys. Lett. 343 (2001) 633–641.
[23] C.M. Tesch, R. de Vivie-Riedle, Phys. Rev. Lett. 89 (2002) 157901.
[24] B.M.R. Korff, U. Troppmann, K.L. Kompa, R. de Vivie-Riedle, J. Chem. Phys. 123 (2005) 244509.
[25] C.M. Tesch, R. de Vivie-Riedle, J. Chem. Phys. 121 (2004) 12158–12168.
[26] U. Troppmann, R. de Vivie-Riedle, J. Chem. Phys. 122 (2005) 154105.
[27] D. Babikov, J. Chem. Phys. 121 (2004) 7577–7585.
[28] Y. Ohtsuki, Chem. Phys. Lett. 404 (2005) 126–131.
[29] S. Suzuki, K. Mishima, K. Yamashita, Chem. Phys. Lett. 410 (2005) 358–363.
[30] I.R. Sola, V.S. Malinovsky, J. Santamaria, J. Chem. Phys. 120 (2004) 10955–10960.
[31] D. Sugny, C. Kontz, M. Ndong, Y. Justum, G. Dive, M. Desouter-Lecomte, Phys. Rev. A 74 (2006) 0434R19.
[32] H.-P. Breuer, F. Petruccione, The Theory of Open Quantum Systems, Oxford University Press, 2002.
[33] U. Weiss, Quantum Dissipative Systems, World Scientific, Singapore, 1999.
[34] L. Wang, H.-D. Meyer, V. May, J. Chem. Phys. 125 (2006) 014102.
[35] H. Wang, J. Chem. Phys. 113 (2000) 9948–9956.
[36] M. Nest, H.-D. Meyer, J. Chem. Phys. 119 (2003) 24–33.
[37] I. Burghardt, M. Nest, G. Worth, J. Chem. Phys. 119 (2003) 5364–5378.
[38] D. Gelman, C.P. Koch, R. Kosloff, J. Chem. Phys. 121 (2004) 661–671.
[39] Y. Ohtsuki, J. Chem. Phys. 119 (2003) 661–671.
[40] Y. Ohtsuki, W. Zhu, H. Rabitz, J. Chem. Phys. 110 (1999) 9825–9832.
[41] R. Xu, Y. Yan, J. Chem. Phys. 116 (2002) 9196–9206.
[42] Y. Mo, R.-X. Xu, P. Cui, Y. Yan, J. Chem. Phys. 122 (2005) 084115.
[43] C. Meier, D.J. Tannor, J. Chem. Phys. 111 (1999) 3365–3376.
[44] N.V. Vitanov, T. Halfmann, B. Shore, K. Bergmann, Annu. Rev. Phys. Chem. 52 (2001) 763–809.
[45] S. Guérin, H.R. Jauslin, Adv. Chem. Phys. 125 (2003) 147–267.
[46] L.P. Yatsenko, V.I. Romanenko, B.W. Shore, K. Bergmann, Phys. Rev. A 65 (2002) 043409.
[47] M. Demirplak, S.A. Rice, J. Chem. Phys. 116 (2002) 8028–8035.
[48] Q. Shi, E. Geva, J. Chem. Phys. 199 (2003) 11773–11787.
[49] P.A. Ivanov, N.V. Vitanov, K. Bergmann, Phys. Rev. A 70 (2004) 063409.
[50] I. Burghardt nad, K.B. Møller, J. Chem. Phys. 117 (2002) 7409–7425.
[51] M. Hartmann, J. Pittner, V. Bonacic-Koutecký, J. Chem. Phys. 114 (2001) 2106–2136.
[52] A.J. Leggett, S. Chakravarty, A.T. Dorsey, M.P.A. Fisher, A. Garg, W. Zwerger, Rev. Mod. Phys. 59 (1987) 1–85.
[53] R. Zwanzig, J. Chem. Phys. 33 (1960) 1338–1341.
[54] I. Burghardt, J. Chem. Phys. 114 (2001) 89–101.
[55] A.G. Redfield, Adv. Magn. Res. 1 (1965) 1–32.
[56] S.G. Schirmer, A.I. Solomon, Phys. Rev. A 70 (2004) 022107.
[57] G. Lindblad, Comm. Math. Phys. 48 (1976) 119–130.
[58] B. Lasorne, G. Dive, D. Lauvergnat, M. Desouter-Lecomte, J. Chem. Phys. 118 (2003) 5831–5840.
[59] C. Altafini, Phys. Rev. A 70 (2004) 062321.
[60] C. Altafini, J. Math. Phys. 44 (2003) 2357–2372.
[61] W. Zhu, J. Bottina, H. Rabitz, J. Chem. Phys. 108 (1998) 1953–1963.
[62] W. Zhu, H. Rabitz, J. Chem. Phys. 109 (1998) 385–391.
[63] Y. Ohtsuki, G. Turicini, H. Rabitz, J. Chem. Phys. 120 (2004) 5509–5517.
[64] K. Sundermann, R. de Vivie-Riedle, J. Chem. Phys. 110 (1999) 1896–1904.
[65] J.P. Palao, R. Kosloff, Phys. Rev. Lett. 89 (2002) 188301.
[66] W.H. Miller, N.C. Handy, J.E. Adams, J. Chem. Phys. 72 (1980) 99–112.
[67] J.M. Bowman, B. Gazdy, J. Chem. Phys. 93 (1990) 1774–1784.
[68] J.C. Light, Z. Bacic, J. Chem. Phys. 87 (1987) 4008–4019.
[69] B. Kuhn, T.R. Rizzo, D. Luckhaus, M. Quack, M.A. Suhm, J. Chem. Phys. 111 (1999) 2565–2587.
[70] S.C. Farantos, J. Tennyson, J. Chem. Phys. 84 (1986) 6210–6217.
[71] B.R. Johnson, W.P. Reinhardt, J. Chem. Phys. 85 (1986) 4538–4556.
[72] D. Lauvergnat, A. Nauts, Y. Justum, X. Chapuisat, J. Chem. Phys. 114 (2001) 6592–6604.
[73] S. Blasco, D. Lauvergnat, Chem. Phys. Lett. 373 (2003) 344–349.
[74] D. Lauvergnat, A. Nauts, Chem. Phys. 305 (2004) 105–113.
[75] X. Chapuisat, C. Saint-Espès, Chem. Phys. 159 (1992) 391–419.
[76] D. Lauvergnat, A. Nauts, J. Chem. Phys., submitted for publication.
[77] D.O. Odero, Eur. Phys. J. D. 19 (2002) 3–8.
[78] D. Lauvergnat, ElVibRot: Quantum Dynamics Code, http://www.lcp.u-psud.fr/Pageperso/lauvergnat.
[79] T. Hornung, S. Gordienko, R. de Vivie-Riedle, B.J. Verhaar, Phys. Rev. A 66 (2002) 043607.
[80] S.E. Sklarz, D.J. Tannor, Rev. A 66 (2002) 053619.
[81] R. Xu, Y. Yan, Y. Ohtsuki, Y. Fujimura, H. Rabitz, J. Chem. Phys. 120 (2004) 6600–6608.
[82] B.J. Sussman, D. Townsend, M.Y. Ivanov, A. Stolow, Science 314 (2006) 278–281.